

# Targeting VEGF-A in an Immunocompetent Orthotopic Mouse Model of Mesenchymal Glioblastoma Improves Antitumorigenicity and Decreases Proinflammatory Response in Normal Brain Tissue after Fractionated Radiotherapy

Alexander Edward Nieto, Daniel Felix Fleischmann, Kristian Unger, Valerie Albrecht, Jessica Maas, Horst Zitzelsberger, Claus Belka, Martin Proescholdt, Kirsten Lauber, Maximilian Niyazi, and Michael Orth\*

Glioblastoma is the most aggressive primary brain tumor characterized by a dismal prognosis and a profound therapy resistance that is most evident for the mesenchymal molecular subtype of glioblastoma. Targeting vascular endothelial growth factor (VEGF)-A by the monoclonal antibody bevacizumab, despite failing to improve survival in randomized trials, yields relevant benefits in glioblastoma patients such as reduction of radionecrosis, an adverse event associated with radiotherapy. This demands for continued research to identify optimal combinations of anti-VEGF-A and standard therapies for glioblastoma treatment. We show here that blocking VEGF-A in an immune competent orthotopic glioblastoma mouse model resembling the adverse mesenchymal molecular subtype increases the tumoricidal effect of computed tomography (CT)-based fractionated radiotherapy and also rectifies irradiation-induced expression of genes with known association to mesenchymal subtype enrichment as revealed by microarray-based transcriptome analyses of explanted tumors. VEGF-A blockade also decreases the expression of myeloid-cell-related gene patterns in irradiated tumors and lowers inflammatory response in normal brain tissue after tumor irradiation. Hence, these data both provide a hint how blockade of VEGF-A increases the effect of radiotherapy in mesenchymal glioblastoma and a mechanistic base for clinical observations reporting reduced incidences of radionecrosis in glioblastoma patients treated with radiotherapy upon concurrent administration of bevacizumab.

## 1. Introduction

Glioblastoma is the most common malignant primary brain tumor in adults with a highly dismal prognosis.<sup>[1]</sup> Standard-of-care comprises resection (when possible) followed by a fractionated radiochemotherapy implementing the alkylating drug temozolomide (TMZ) and a maintenance therapy again implementing TMZ.<sup>[2]</sup> Based on cytogenetic and transcriptomic profilings, glioblastoma has been divided into three distinct molecular subtypes: a proneural, a classical, and a mesenchymal subtype,<sup>[3,4]</sup> the latter of which exhibiting the highest resistance to therapy.<sup>[5,6]</sup>

Since glioblastoma represents a hyperemic type of tumor characterized by a strong upregulation and hyperactivation of vascular endothelial growth factor (VEGF) and hypoxia-inducible factor (HIF) signaling, the VEGF-A-targeting antibody bevacizumab (e.g., Avastin)<sup>[7]</sup> was originally considered a promising candidate for improve of glioblastoma treatment efficacy.<sup>[8]</sup> However, bevacizumab, despite improving

 The ORCID identification number(s) for the author(s) of this article can be found under <https://doi.org/10.1002/adtp.202400374>

© 2025 The Author(s). Advanced Therapeutics published by Wiley-VCH GmbH. This is an open access article under the terms of the [Creative Commons Attribution](https://creativecommons.org/licenses/by/4.0/) License, which permits use, distribution and reproduction in any medium, provided the original work is properly cited.

DOI: 10.1002/adtp.202400374

A. E. Nieto, D. F. Fleischmann, K. Unger, V. Albrecht, J. Maas, C. Belka, K. Lauber, M. Niyazi, M. Orth  
 Department of Radiation Oncology  
 LMU University Hospital  
 LMU Munich  
 81377 Munich, Germany  
 E-mail: [michael.orth@med.uni-tuebingen.de](mailto:michael.orth@med.uni-tuebingen.de)  
 D. F. Fleischmann, K. Unger, C. Belka, K. Lauber, M. Niyazi  
 German Cancer Consortium (DKTK)  
 Munich Partner Site  
 80336 Munich, Germany  
 D. F. Fleischmann  
 German Cancer Research Center (DKFZ)  
 69120 Heidelberg, Germany

progression-free survival (PFS) of glioblastoma patients,<sup>[9–13]</sup> failed to enhance overall survival (OS) in randomized trials, both in conjunction with radio(chemo)therapy and lomustine,<sup>[9–11,13]</sup> precluding its approval for both, first- and second-line treatment of glioblastoma.<sup>[14]</sup> However, these trials demonstrated several beneficial effects for bevacizumab besides prolongation of PFS such as reduced corticosteroid dependence, relieved edema, and reduced incidence of adverse events associated with standard therapies such as radiation-induced necrosis (radionecrosis).<sup>[9,10,15]</sup> Further studies, however, swiftly showed that only subsets of glioblastoma patients benefitted from bevacizumab and the reasons for that remained unclear so far.<sup>[16]</sup> Stratification of glioblastoma patients to molecular subtypes of their tumors yielded conflicting or negative results,<sup>[12,17,18]</sup> and biomarkers for VEGF-A-targeting therapy in glioblastoma are still far from clinical maturity.<sup>[19]</sup> Nevertheless, the benefit of bevacizumab, e.g., when combined with radiotherapy, are unquestioned, both in the primary and the recurrent setting.<sup>[9,10,20,21]</sup> This demands for continued research, both on the preclinical as on the clinical level to identify patient populations that benefit from bevacizumab as well as biomarkers that are of predictive value for responses to VEGF-A-targeting therapy in glioblastoma patients.

Using an immunocompetent orthotopically implanted glioblastoma mouse model based on the widely used mouse glioblastoma cell line GL261<sup>[22]</sup> and assigned to the adverse mesenchymal subtype of glioblastoma, we show that targeting VEGF-A cannot only improve the tumoricidal effect of fractionated irradiation in mesenchymal glioblastoma, but also prevent the enrichment of mesenchymal subtype-associated gene expression patterns in response to irradiation thereby,

most likely, interfering with proneural–mesenchymal transition, a well-known complication of fractionated radiotherapy in glioblastoma.<sup>[5]</sup> By comparing transcriptomes of irradiated tumors with curated gene sets of different myeloid cell entities, we also can show that radiation-induced enhancement of myeloid cell infiltration into glioblastoma tumors is largely diminished by VEGF-A targeting. Finally, we show that targeting VEGF-A reduces inflammatory signaling and thus high levels of myeloid cell infiltration into nontumorigenic brain tissue upon exposure to irradiation, providing a potential mechanism for how concurrent clinical targeting of VEGF-A, e.g. by bevacizumab, lowers the incidences of radionecrosis in glioblastoma patients treated with radiotherapy.<sup>[20,23–25]</sup>

## 2. Results

### 2.1. Orthotopically Implanted GL261 Tumors Recapitulate the Mesenchymal Subtype of Human Glioblastoma

To investigate the effects of pharmacologically targeting VEGF-A on glioblastoma response to fractionated radiotherapy, we took advantage of the GL261 glioblastoma mouse model system.<sup>[22]</sup> Immunocompetent C57BL/6 mice were intracranially inoculated with 90 000 GL261 cells as previously described,<sup>[26]</sup> and tumors were allowed to grow for time intervals of 7–12 days. To decipher the molecular subtype of these tumors, tumor-carrying control mice were sacrificed at day 12 after inoculation and tumors as well as nontumorigenic brain tissue from contralateral hemispheres were explanted. Total RNA was extracted both from tumors and from normal brain tissue and subjected to transcriptomic analyses (Table S1, Supporting Information). As expected, significant differences were found in global mRNA expression of tumors when compared to normal brain tissues as revealed by both, unsupervised hierarchical clustering analysis depicting the 100 most upregulated and downregulated genes in tumors and principal component analysis (PCA, Figure S1A,B, Supporting Information). To identify the molecular subtype of human glioblastoma GL261 tumors mostly corresponded to, we used transcriptome data from glioblastoma patients provided by The Cancer Genome Atlas (TCGA).<sup>[27]</sup> We first compared the transcriptomes from patient tumors corresponding to each molecular subtype<sup>[3,4]</sup> (Figure S2A, Supporting Information) and found that indeed transcriptomes from different molecular subtypes clustered apart from each other when analyzed by PCA (Figure S2B, Supporting Information), yielding 35.5% of variance in the first dimension (PC1) and 24.7% in the second (PC2). We next performed Kyoto encyclopedia of genes and genomes (KEGG) pathway<sup>[28]</sup> and gene set enrichment analysis (GSEA)<sup>[29]</sup> followed by manual assignment of the pathways we identified as upregulated or downregulated to cellular processes/networks such as cell cycle regulation, DNA replication or immune signaling (Figure 1A; Table S2, Supporting Information). For each subtype, we used the five most representative patients within the TCGA cohort which were identified by PCA (Figure S1B, Supporting Information). This approach yielded highest percentages for cell cycle regulation, DNA damage repair, and cell death, and this was most evident for tumors of the classical and the proneural subtype. Tumors of the mesenchymal subtype, in addition, also showed a strong upregulation of pathways involved in

---

K. Unger, H. Zitzelsberger  
Research Unit Translational Metabolic Oncology  
Helmholtz Center Munich  
German Research Center for Environmental Health GmbH  
85764 Neuherberg, Germany

K. Unger, H. Zitzelsberger, C. Belka, K. Lauber  
Clinical Cooperation Group “Personalized Radiotherapy in Head and Neck Cancer” Helmholtz Center Munich  
German Research Center for Environmental Health GmbH  
85764 Neuherberg, Germany

K. Unger, C. Belka, M. Niyazi  
Bavarian Cancer Research Center (BZKF)  
91012 Munich, Germany

M. Proescholdt  
Department of Neurosurgery  
Regensburg University Hospital  
93053 Regensburg, Germany

M. Niyazi  
German Cancer Consortium (DKTK)  
Tübingen Partner Site  
72076 Tübingen, Germany

A. E. Nieto  
III. Medical Department for Hematology and Oncology  
University Hospital rechts der Isar  
Technical University Munich  
81675 Munich, Germany

M. Niyazi, M. Orth  
Department of Radiation Oncology  
University Hospital Tübingen  
72076 Tübingen, Germany

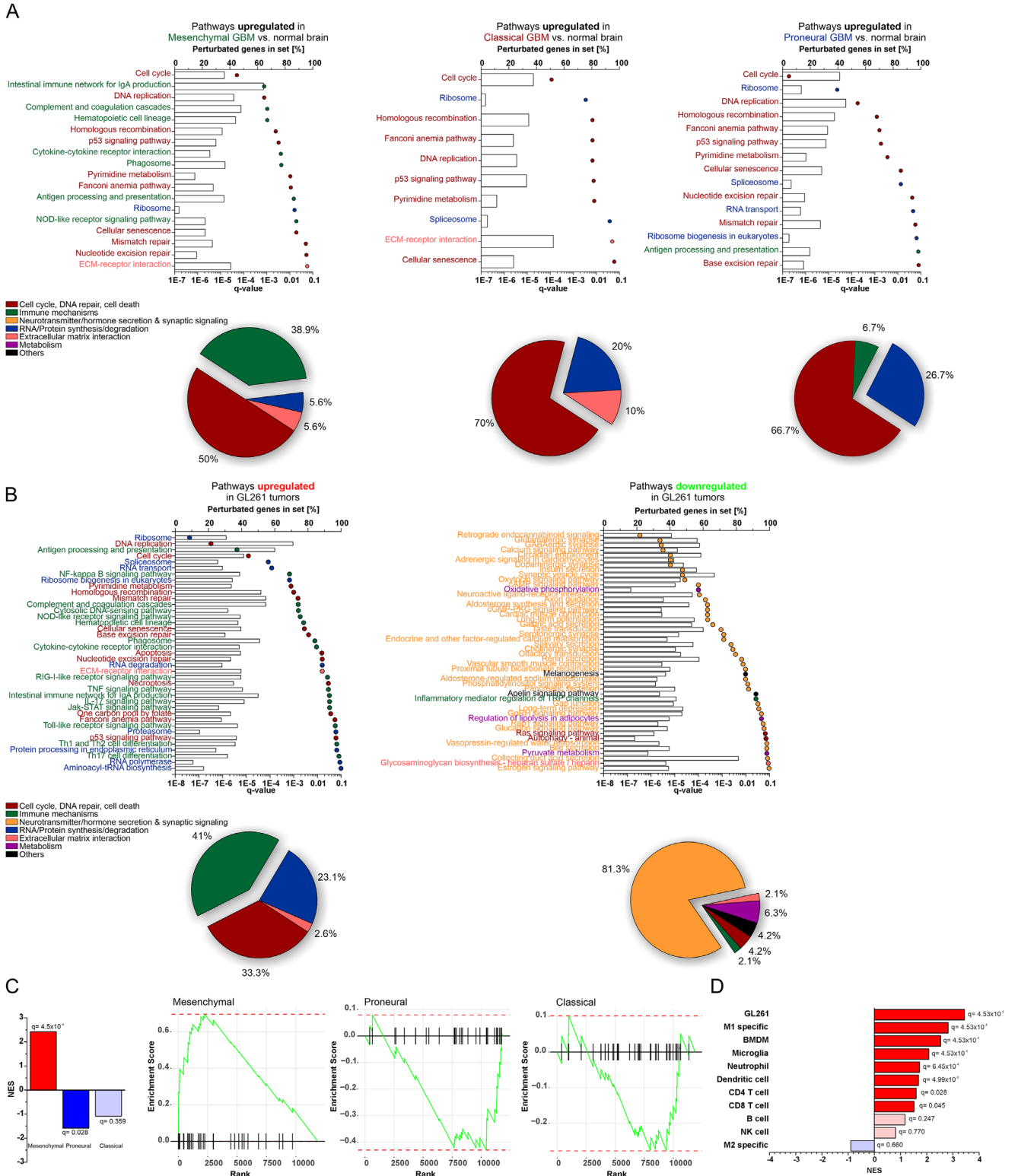


**Figure 1.** The syngenic orthotopic GL261 glioblastoma mouse model mostly recapitulates the mesenchymal subtype of glioblastoma. A) KEGG pathway analysis followed by GSEA of upregulated gene sets in human glioblastoma samples of each molecular subtype as deposited in the TCGA database (top). Proportions of perturbed genes per set (bars with percentages) and corresponding *q*-values (indicated by dots, cutoff  $\leq 0.1$ ) are shown. Percentages of cellular processes encompassing identified pathways with portions of upregulation in the five most representative patients of each subtype are shown at the bottom. B) KEGG pathway analysis followed by GSEA of upregulated (left) and downregulated (right) gene sets in GL261 tumors explanted from control mice ( $n = 4$ ) at day 12 after inoculation when compared to normal brain tissue isolated from contralateral hemispheres ( $n = 4$ ) (top) and

immunogenic signaling and the innate immune response which was quite expected since high infiltration by myeloid cells is a documented hallmark of mesenchymal brain tumors.<sup>[30,31]</sup> We then performed similar analyses using the transcriptome data we obtained for GL261 tumors and normal mouse brain (Figure 1B; Figure S1C and Table S3, Supporting Information). The percentages of processes/networks encompassing upregulated KEGG pathways in GL261 tumors showed a high similarity to those we obtained for human mesenchymal tumors (Figure 1A,B) so far implying that GL261 tumors might indeed resemble this specific subtype of glioblastoma.

To further substantiate that GL261 tumors indeed resembled mesenchymal glioblastoma, we performed GSEA calculating gene set enrichment scores (ESs) for each subtype and normalized these to the differences in size of the gene sets (normalized enrichment scores (NESs)). Again, we found highest enrichments for gene sets with association to the mesenchymal subtype while gene sets associated with the proneural and the classical subtype were deriched (Figure 1C; Table S5, Supporting Information) confirming that orthotopic GL261 tumors, when implanted into immunocompetent C57BL/6 mice, indeed resembled human mesenchymal glioblastoma, at least on the transcriptional level. In addition, we detected a strong upregulation of pathways associated with immune response in GL261 tumors (Figure 1B) which was consistent with reports for mesenchymal human glioblastoma showing a strong infiltration of these tumors by different, mostly immunosuppressive populations of myeloid cells.<sup>[30,31]</sup> To gain insight into the populations of immune cells that infiltrated GL261 tumors, we curated customized gene sets for different leukocyte entities (Table S4, Supporting Information),<sup>[32,33]</sup> calculated NESs, and compared those with the values obtained for GL261 tumors (Figure 1D). Interestingly, GL261 tumors showed a similar pattern of NESs as M1-polarized macrophages, bone marrow-derived monocytes (BMDMs), microglia, and neutrophils, as well as to lesser extents, as those found for dendritic cells and CD4<sup>+</sup> or CD8<sup>+</sup> T cells. This fitted with previously published data on human mesenchymal glioblastoma showing increased infiltration of this type of tumor by myeloid cell populations similar to those showing highest correspondence in NESs identified in our GL261 tumors<sup>[30,31]</sup> (Figure 1D). Therefore, we concluded that GL261-derived tumors generated by intracranial implantation into immunocompetent C57BL/6 mice resembled the mesenchymal subtype of human glioblastoma providing an excellent model to preclinically study this highly refractory glioblastoma subtype.<sup>[5,34]</sup>

## 2.2. Targeting VEGF-A Ameliorates Fractionated Radiotherapy in the Mesenchymal Subtype-Resembling GL261 Glioblastoma Mouse Model

Having established that orthotopic GL261 tumors in immunocompetent mice mostly resembled the mesenchymal subtype of

human glioblastoma, we next assessed what impact the blockade of VEGF-A would exhibit on response to fractionated radiotherapy in this resistant preclinical glioblastoma mouse model. Mice carrying GL261 tumors were treated by cone beam computed tomography (CBCT)-based fractionated radiotherapy (10 × 2 Gy) and concurrent administration of the murine VEGF-A-specific antibody G6-31<sup>[35]</sup> (3 × 0.1 mg) over 2 weeks (Figure 2A–C). A positive effect for abrogating VEGF signaling in concurrence with radiotherapy has been shown in preclinical glioblastoma models before,<sup>[36–38]</sup> yet not with regard to glioblastoma subtypes, and not in a near-clinical irradiation setting as it was used here. Co-administration of G6-31 resulted in a delay of tumor progression (Figure 2C,E; Table S6, Supporting Information), and also in significantly longer survival when compared to each treatment modality for its own (Figure 2D). G6-31 administered as monotherapy elongated the median survival from 14 days for control mice to 21 days, while sole radiotherapy yielded a prolongation till day 23 (Figure 2D). However, the combination of both treatment modalities prolonged the median survival up to 32 days which was significantly longer when compared to controls and single treatments suggesting that VEGF-A blockade can compromise the intrinsically high levels of treatment resistance in mesenchymal glioblastoma,<sup>[5,6]</sup> at least to some extent. This is also remarkable with respect to other reports showing that the mesenchymal subtype exhibits resistance to both, radiotherapy and VEGF-A-targeting therapy,<sup>[5,39,40]</sup> implying that combinatorial effects between these two modalities should rather be mild or even absent when tested in a preclinical glioblastoma model resembling this subtype.

## 2.3. Targeting VEGF-A Reduces the Expression of Mesenchymal Subtype-Related Gene Sets Both in Monotherapy Setting and in Combination with Radiotherapy

The unexpectedly strong effect on the outcome of the mesenchymal glioblastoma-resembling GL261 mouse model after fractionated radiotherapy (Figure 2) elicited by the co-administration of G6-31 prompted us to examine whether blockade of VEGF-A signaling affects the molecular subtype composition in tumors exposed to fractionated irradiation (Figure 3). In glioblastoma patients, fractionated radiotherapy was shown to induce a transition from the proneural to the mesenchymal subtype, and this transition coincided with a strong increase in radioreistance of their tumors.<sup>[5,39]</sup> We therefore tested whether exposure of orthotopic GL261 tumors to fractionated radiotherapy results in an enrichment of mesenchymal subtype-associated gene set expression when compared to vehicle-treated tumors (Figure 3A). Intriguingly, this proved to be true confirming that mesenchymal transition in glioblastoma tumors upon treatment with fractionated irradiation could indeed be reconstituted in our model. We calculated the respective proportions of normalized subtype-specific gene expression (NESs) in explanted tumors

percentages of processes encompassing these pathways with portions of upregulation. C) Normalized enrichment scores (NESs) for gene sets related to all three molecular subtypes<sup>[4]</sup> as revealed by GSEA and expressed in GL261 tumors explanted at day 12 after inoculation. D) NESs of GL261 tumors and different entities of myeloid cells as calculated on the basis of customized gene sets (Table S4, Supporting Information) curated from microarray data of the ImmGen project (GSE15907 and GSE37448).<sup>[32]</sup> M1/M2-polarized macrophages were discriminated on the basis of curated gene sets with maximal distance between M1/M2 polarization,<sup>[33]</sup> generated by non-negative matrix factorization (NMF).

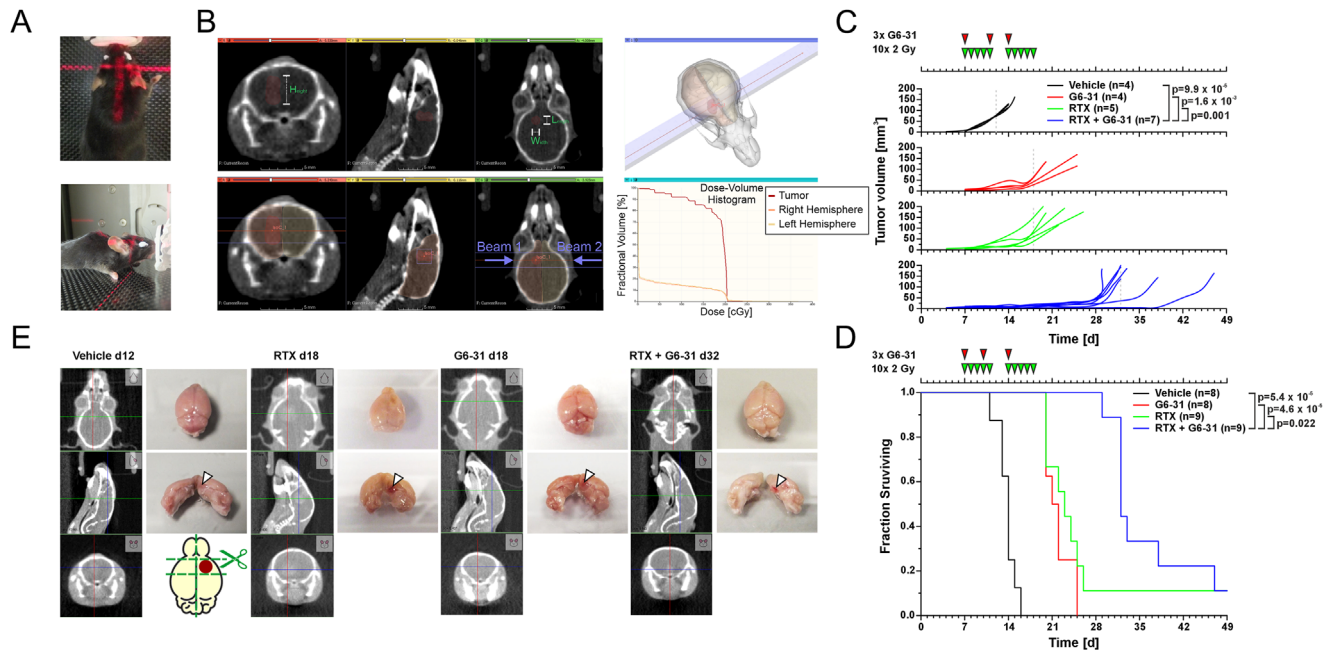


**Figure 2.** VEGF-A targeting by G6-31 improves the effect of fractionated radiotherapy in the GL261 glioblastoma mouse model. A) Photographs depicting positioning of mice using laser-guidance. B) Monitoring of tumors and treatment planning. Axial, sagittal, and coronary CBCTs with GTV delineation (top) and beam geometry (bottom) are shown. C) Tumor growth over time. Mice were irradiated at 2 Gy of dose at days 7–11 and 14–18, and 0.1 mg G6-31 was administered intraperitoneally at days 7, 11, and 14 (shown on top). Growth curves are depicted as spline regressions from top to bottom for control mice (vehicle, black,  $n = 4$ ), G6-31-treated mice (red,  $n = 4$ ), radiotherapy (RTX) Wingless/Integrated-treated mice (green,  $n = 5$ ), and combined treated mice (blue,  $n = 7$ ). Tumor growth was measured twice weekly by contrast-enhanced CBCT starting at day 7 after inoculation. Tumor volumes were calculated by measuring the lengths, widths, and heights along orthogonal axes<sup>[26]</sup> (see panel (B)) and group comparisons were performed by two-way analysis of variance (ANOVA). Time points of tumor explantation are depicted by gray dotted lines. D) Kaplan–Meier survival curve analysis for all treatment groups (vehicle  $n = 8$ , G6-31  $n = 8$ , RTX  $n = 9$ , RTX + G6-31  $n = 9$ ). Significances were calculated by log-rank test with Bonferroni–Holm correction. E) CBCT scans with isocenters and explanted brains from mice of the vehicle group (left, day 12), the RTX group (day 18), the G6-31 group (day 18), and the RTX + G6-31 group (right, day 32). Tumors and associated edema are marked by arrowheads. The schematic illustrates the geometry of surgical sample collection.

either treated by sole radiotherapy, sole VEGF-A blockade or the combination thereof, and compared those NESs to the respective expression levels we obtained for vehicle-treated controls. Sole irradiation, again, resulted in a strong induction of mesenchymal subtype-associated signature gene expression while decreasing those expression patterns with relations to the proneural and the classical subtype (Figure 3A). G6-31, however, largely decreased the expression of mesenchymal subtype-associated gene sets, both when applied in monotherapy setting as upon combination with radiotherapy (Figure 3B), implying that concurrent blockade of VEGF-A can indeed interfere with mesenchymal enrichment during course of a fractionated radiotherapy. To substantiate this, we also looked for immune cell-specific gene set expression patterns in GL261 tumors either exposed to radiotherapy, G6-31, or their combination. Sole irradiation, as expected, resulted in a strong increase of myeloid cell-specific gene expression patterns (Figure 3C) with patterns resembling those of BMDMs, M1-polarized macrophages, microglia, neutrophils, natural killer (NK), cells and dendritic cells being most prominent. Single G6-31 treatment, to the contrary, yielded a strong suppression in expression of most of these gene sets, and this was also evident for gene sets corresponding to immune cell entities of immunosuppressive function such as M2-polarized macrophages<sup>[41]</sup> (Figure 3C; Table S7, Supporting Information).

Cells involved in the adaptive immune response, to the contrary, particularly CD4<sup>+</sup> and CD8<sup>+</sup> T cells, were mostly unaffected by G6-31 treatment and this pattern was also seen when G6-31 was combined with irradiation (Figure 3C; Table S7, Supporting Information). From these data we concluded that targeting VEGF-A in mesenchymal glioblastoma might be a promising strategy to accelerate the tumoricidal effect of fractionated irradiation in this refractory subtype and also provides an opportunity to interfere with both treatment-induced proneural–mesenchymal transition<sup>[5]</sup> and enhanced infiltration of tumors by immunosuppressive myeloid cells.

#### 2.4. Blocking VEGF-A Reduces Proinflammatory Signaling in Irradiated Normal Brain Tissue

A repeatedly documented benefit of bevacizumab when co-administered in concurrence with radiotherapy in glioblastoma patients is the reduction in incidence of necrosis of non-neoplastic parenchyma receiving dose exposures (radionecrosis).<sup>[20,23–25]</sup> The reason for this effect is still unclear which is why we decided to ask how blocking VEGF-A signaling by G6-31 affects non-neoplastic mouse brain tissue upon similar treatment as GL261 tumors (Figure 4). We therefore

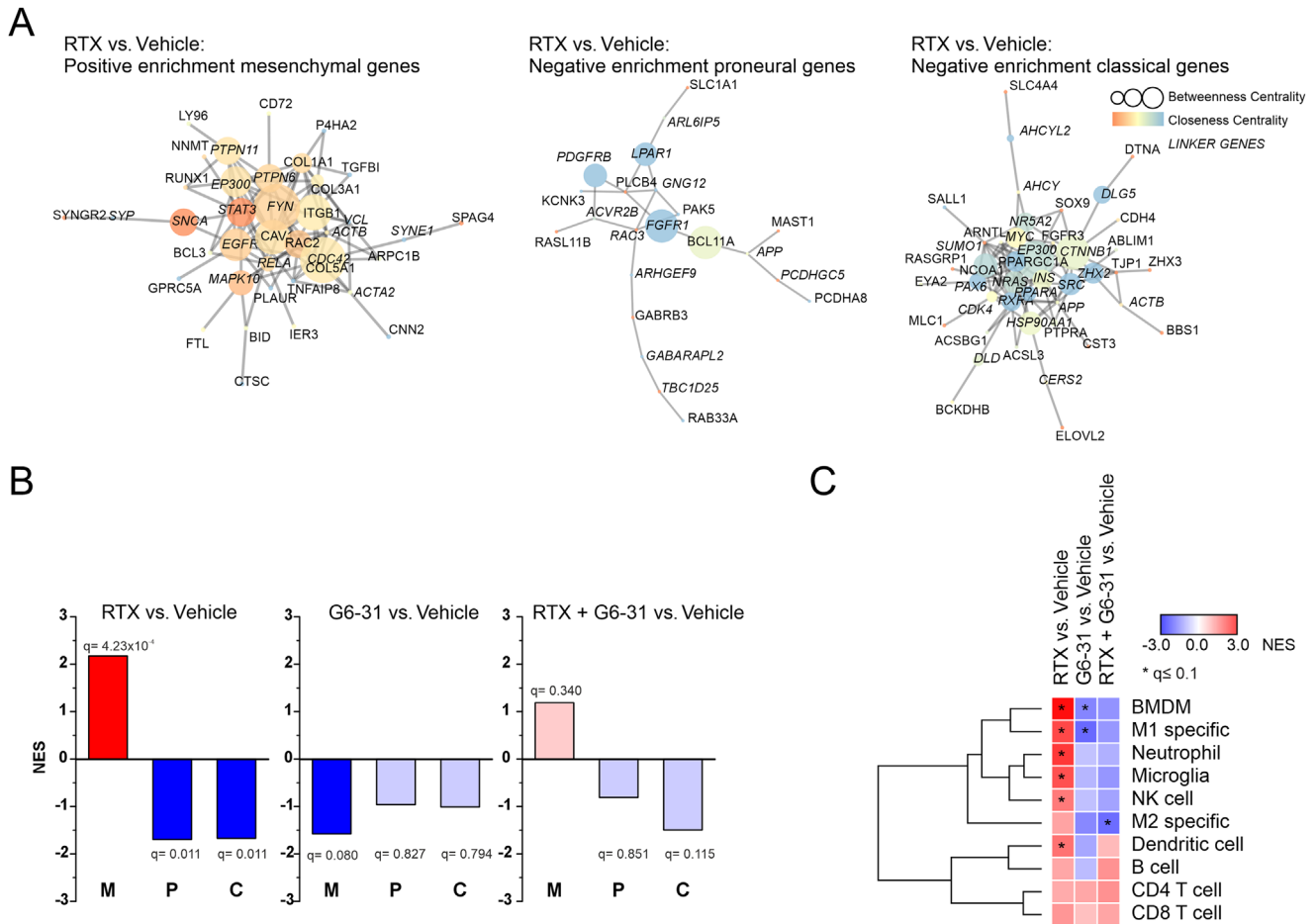


**Figure 3.** VEGF-A targeting by G6-31 reduces the propensity of mesenchymal subtype-specific gene set expression in GL261 tumors and alters the immunogenic tumor microenvironment. A) Functional interaction networks of leading-edge genes in GL261 tumors upon treatment with radiotherapy (RTX,  $n = 3$ ) when compared to control-treated tumors (“vehicle,”  $n = 4$ ). Networks depicting genes with positive enrichment in mesenchymal tumors and negative enrichments in proneural and classical tumors (from left to right) are shown. Importance (“betweenness”) is shown by circle sizes and “closeness” is depicted by color. B) NESs corresponding to mesenchymal (M), proneural (P), and classical (C) tumors calculated for GL261 tumors that were treated by sole RTX (left,  $n = 3$ ), G6-31 (middle,  $n = 4$ ), and RTX + G6-31 (right,  $n = 3$ ) when compared to control-treated tumors (“vehicle,”  $n = 4$ ). C) Hierarchical clustering of NESs obtained for different immune cell populations in RTX-treated, G6-31-treated, and RTX + G6-31-treated GL261 tumors.  $q$ -values with a cut-off  $\leq 0.1$  are indicated by asterisks.

treated mice with right-striatal GL261 tumors by CT-based fractionated radiotherapy ( $2 \times 5 \times 2$  Gy) with two opposing fields adopting a contralateral beam geometry that yields equal dose distributions between both hemispheres (Figure 2B, right) resulting in a 2 Gy exposure per fraction of both, the tumor and 10% of the left hemisphere. We then analyzed symmetrically explanted left striatal brain tissue (Figure 2E, schematic) by microarray followed by GSEA and calculation of NESs as before (Figure 3). Irradiation alone, as expected, resulted in strong enrichment of pathways associated with inflammatory responses such as interleukin-2 (IL-2)-signal transducer and activator of transcription 5 (STAT5) signaling, allograft rejection, coagulation, complement activation, tumor necrosis factor alpha (TNF $\alpha$ ) signaling, interleukin-6 (IL-6)-Janus kinase (JAK) signal transducer and activator of transcription 3 (STAT3) as well as interferon (IFN) alpha (IFN $\alpha$ ) and gamma (IFN $\gamma$ ) signaling (Figure 4A,B; Table S8, Supporting Information). Notably, most of these gene sets were much less expressed when mice were

additionally treated with G6-31 indicating that inflammatory responses to fractionated irradiation and thus, presumably, radiation-induced necrotic events in normal brain tissues can indeed be diminished by VEGF-A blockade, providing a strong hint to the immunological basis of mitigation of radionecrosis in radiotherapy-treated glioblastoma patients treated with bevacizumab.<sup>[20,23–25]</sup> However, several proinflammatory pathways also remained unaltered in brains from mice treated by radiotherapy and G6-31 when compared to mice treated by sole irradiation (Figure 4A). We therefore performed a signaling pathway enrichment using experimental datasets 2 (SPEED2) analysis<sup>[42]</sup> to compare the activation of inflammatory signaling cascades in brains from mice solely treated with radiotherapy with those from mice receiving radiotherapy and VEGF-A blockade (Figure 4C). This analysis confirmed a higher upregulation of inflammatory signaling pathways such as interleukin-1 (IL-1), JAK-STAT, Toll-like receptor (TLR), and TNF $\alpha$  in mice receiving sole radiotherapy when compared to doubly treated mice, but

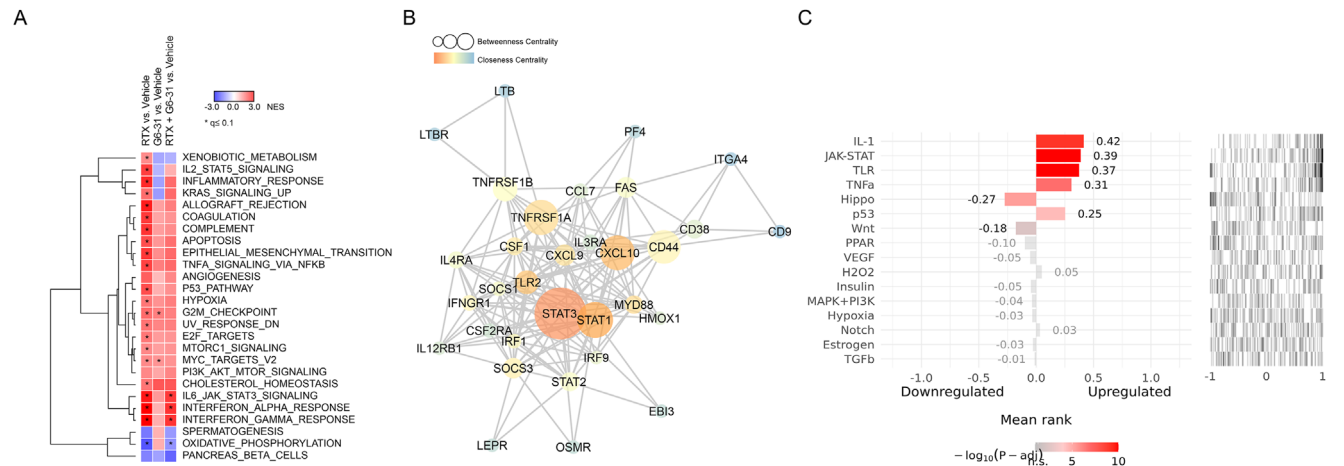


**Figure 4.** VEGF-A targeting reduces radiation-induced inflammatory signaling in normal brain tissue. **A**) Hierarchical clustering of NESs derived from GSEA performed on normal tissue from mouse brains treated with RTX ( $n = 3$ ), G6-31 ( $n = 5$ ), and RTX+G6-31 ( $n = 3$ ) and compared to control-treated brains (“vehicle,”  $n = 4$ ).  $q$ -values with a cutoff of  $\leq 0.1$  are indicated by asterisks. **B**) Functional interaction network of the leading edge intersect HALLMARK\_IL6\_JAK\_STAT3\_SIGNALING pathway gene set as identified by GSEA comparing MSigDB hallmarks<sup>[49]</sup> between RTX and RTX+G6-31-treated brains. **C**) SPEED2 analysis of inflammatory human genes homologous to respective mouse genes in RTX ( $n = 3$ ) and RTX+G6-31-treated brains ( $n = 3$ ), and ranked by the levels of upregulation and downregulation.  $q$ -values with a cutoff of  $\leq 0.1$  are indicated by asterisks and fold change threshold is  $>2$ .

also showed a downregulation of other immune response-related pathways such as Hippo and Wingless and Int-1 (WNT) (Figure 4C). Since astrocytes are known to secrete numerous cytokines involved in radiation-induced inflammation of neuronal tissue as well as high levels of VEGF-A upon irradiation<sup>[43,44]</sup> resulting in various downstream events that can all contribute to necrosis formation,<sup>[45–47]</sup> we assume that most of the effects observed here are mediated via sequestration of VEGF-A secreted by astrocytes in response to irradiation. Similarly, astrocytes were also shown to actively contribute to mesenchymal transition and consequent acceleration of therapy resistance by regulating neuroinflammatory processes in response to different insults including therapy.<sup>[48]</sup> Thus, we suggest that pharmacological VEGF-A targeting indeed mostly acts by affecting gene pattern expression in astrocytes, rather than in other cell entities, although this has to be shown by future studies.

### 3. Discussion

Glioblastoma, despite all efforts, remains a devastating disease with poor prognosis urging for rapid improvement of currently available treatment options. Radiotherapy is a cornerstone in glioblastoma treatment,<sup>[50]</sup> yet its efficacy is limited, both as a monotherapy as in combination with TMZ.<sup>[51,52]</sup> In addition, cranial radiotherapy is frequently associated with adverse events such as radionecrosis, a condition that can cause brain edema and even progress to sensorimotor and other neurological deterioration reducing patient life quality and limiting administration of full doses as well.<sup>[53]</sup> The clinical impact of VEGF-targeting therapy, particularly of the VEGF-A-specific antibody bevacizumab on glioblastoma treatment is still unclear.<sup>[54]</sup> On the one hand, bevacizumab failed to prolong OS in randomized trials and upon combination with different treatment modalities including radiotherapy,<sup>[9–11,20]</sup> on the other hand, multiple studies showed a clear benefit for addition of bevacizumab to ra-

diotherapy when analyzing treatment-related adverse events, radionecrosis in particular.<sup>[20,23–25]</sup>

We preclinically investigated the effect of concurrent VEGF-A blockade on the outcome after fractionated radiotherapy ( $2 \times 5 \times 2$  Gy) in an immunocompetent orthotopic glioblastoma mouse model based on the GL261 cell line.<sup>[22]</sup> By comparing the transcriptomes of tumors with those obtained for normal brain tissue explanted from contralateral hemispheres of respective tumor-carrying mice and also with TCGA data from patients suffering from glioblastoma tumors of all three molecular glioblastoma subtypes,<sup>[3,4]</sup> we could assign this syngeneic mouse model to the highly adverse mesenchymal subtype of human glioblastoma (Figure 1). Using this model system, we could then show that blockade of VEGF-A signaling by a mouse VEGF-A-specific antibody increases the effect of fractionated radiotherapy in mesenchymal glioblastoma (Figure 2) which is in line with previous reports showing similar findings for VEGF-A blockade and radiotherapy in glioblastoma mouse models.<sup>[36–38]</sup> However, since these studies employed mice that were immune compromised no further comparison between these data and ours is possible, particularly when coming to inflammatory signaling and myeloid cell infiltration, two signature hallmarks of high-grade mesenchymal brain tumors.<sup>[30,31]</sup> By transcriptome-based assignment of GL261 tumors to the mesenchymal subtype of human glioblastoma (Figure 1) we can show not only a superiority for fractionated radiotherapy and concomitant VEGF-A blockade in this treatment-refractory subtype (Figure 2), but also that targeting VEGF-A can interfere with both, mesenchymal enrichment and myeloid cell infiltration upon irradiation thereby, most likely, abrogating the intrinsically high levels of radioresistance of this subtype (Figure 3).<sup>[5,6]</sup> Despite preclinical data indicating that the combination of VEGF-A blockade and radiotherapy can improve the prognosis of glioblastoma in general and, more specifically, of mesenchymal glioblastoma, clinical evidence shows clearly the opposite negating beneficial effects in terms of

OS both for this molecular subtype<sup>[12,18]</sup> as for the others.<sup>[17,18]</sup> Elucidating the reasons for this discrepancy between preclinical and clinical data clearly requires further research. One possible explanation could be the artificial character of stereotactically inoculated glioblastoma mouse models as deployed here since these models not only are known for their dependence on high angiogenesis levels and, thus, on high levels of VEGF-A,<sup>[55,56]</sup> but also for their limitations, in our case, e.g., resulting in sacrificial and explantation of tumors at different time points when related to therapy as a consequence of differences in tumor progression (Figure 2C).

Some studies, however, clearly showed clinical benefit for bevacizumab when administered in patients suffering from recurrent glioblastoma,<sup>[15,57]</sup> which, at first sight, would fit in terms that recurrent tumors are mostly mesenchymal.<sup>[58,59]</sup> Yet these studies either tested bevacizumab as monotherapy or in combination with irinotecan,<sup>[15,57]</sup> rather than with radiotherapy. Recently, first studies were published which tested bevacizumab together with re-irradiation in recurrent glioblastoma patients.<sup>[20,21,60,61]</sup> However, several aspects in study design such as selection of patients primarily treated with bevacizumab in a monotherapy setting while showing recurrent progress<sup>[61]</sup> as well as the failure of the RTOG1205 trial in proving prolonged OS in recurrent patients treated with bevacizumab or bevacizumab and radiation<sup>[20]</sup> argue against a synergistic or additive tumoricidal effect between these two modalities. Instead, the beneficial effects, most presumably, are merely due to the mitigation of adverse events elicited by re-irradiation in those patients such as radionecrosis and this, in fact, was shown by recently published reports.<sup>[24,60]</sup> In addition, the reduction of radionecrosis upon bevacizumab addition was also observed in the first-line setting<sup>[23,25]</sup> implying a radioprotective role for bevacizumab in patients experiencing radionecrosis as an adverse effect of radiotherapeutic attendance. However, the mechanism(s) underlying this benefit are still unknown, both aggravating patient stratification and improve of current treatment regimens, for example, in terms of dose escalation. By transcriptome analysis and subsequent GSEA and SPEED2 analyses examining the inflammatory gene set expression in non-neoplastic murine brain tissue treated with fractionated radiotherapy, we can show that inflammatory signaling, especially the expression of immunostimulatory cytokines such as IL-1, TLR, and TNF $\alpha$  is strongly increased in normal brain tissue upon irradiation and this effect was significantly mitigated when the VEGF-A-specific antibody G6-31 was co-administered. Our data therefore provide a preclinical hint of how the addition of bevacizumab to radiotherapy in glioblastoma patients modulates the immunogenic tumor microenvironment in response to radiation, both by diminishing the expression of cytokines, most likely by astrocytes,<sup>[62,63]</sup> thus avoiding enhanced infiltration of irradiated normal brain tissue by inflammatory cells (Figure 4) resulting in inflammation and, most presumably, radionecrosis. However, further evidence is needed in order to fully confirm this assumption such as immunohistochemistry staining of myeloid cell populations revealing in fact reduced infiltration of normal brain tissues upon G6-31 treatment by those cells. Yet our data nonetheless should provide a valuable input for further development of clinical regimens implementing VEGF-A-targeting therapies in the radiotherapeutic attendance of primary and recurrent glioblastoma and probably also of brain metastases derived from other malignancies

as recently published studies revealed similar benefits in those patients.<sup>[64–67]</sup>

## 4. Conclusion

Incorporation of the VEGF-A-specific humanized antibody bevacizumab into standard therapy of glioblastoma yields clear clinical benefit, particularly when combined with radiation therapy, demanding for further research to identify synergies between VEGF-A blockade and standard-of-care glioblastoma therapy. We here provide preclinical evidence that targeting VEGF-A is a versatile approach to yield improved outcome after fractionated radiotherapy in mesenchymal glioblastoma, and also to reduce inflammatory signaling and myeloid cell infiltration of tumors and non-neoplastic brain tissue upon irradiation, the latter providing a rationale for the reduced incidence of radionecrosis seen in glioblastoma patients concurrently treated with radiotherapy and bevacizumab.

## 5. Experimental Section

**Cell Lines and Reagents:** The mouse glioblastoma cell line GL261<sup>[22]</sup> was purchased from the National Cancer Institute (NCI, Bethesda, MD, USA) and cultured in Dulbecco's modified Eagle medium (D-MEM) supplemented with 10% fetal calf serum (FCS), 100 U mL<sup>-1</sup> penicillin and 0.1 mg mL<sup>-1</sup> streptomycin (all from ThermoScientific, Schwerte, Germany) at 37 °C and 7.5% CO<sub>2</sub> as previously described.<sup>[68]</sup> Cells were tested for mycoplasma infection on a regular basis using the MycoAlert test kit (Lonza, Cologne, Germany). The mouse VEGF-A-specific monoclonal antibody G6-31<sup>[35]</sup> was obtained from Roche Pharmaceuticals (Penzberg, Germany). It recognizes a VEGF-A epitope that is conserved between human and mouse and overlaps with the receptor binding surface.

**Orthotopic Glioblastoma Mouse Model:** All animal experiments were performed in accordance to the Federation of European Laboratory Animal Science Associations (FELASA) guidelines and upon approval by the "Regierung von Oberbayern" (Munich, Germany, approval number 55.2-1-54-2532-80-14). Briefly, female C57BL/6 mice were obtained from Charles River (Sulzfeld, Germany) and housed in groups of four animals in individually ventilated cages (IVC, Tecniplast, Hohenpeißenberg, Germany) placed inside a specified pathogen-free animal facility with a 12 h day/night cycle. Standard rodent feed (from Sniff, Soest, Germany) and water were provided ad libitum. Inspection of animals was performed on a daily basis and sacrificial was performed when predefined health scores including alteration in hygiene behavior,  $\geq 20\%$  body weight loss, ulcerating wounds, flattened breathing, epileptic seizures or spasms, paralysis of extremities, bloody diarrhea, apathy, hunched posture or self-mutilation were met. To generate orthotopic glioblastoma tumors, mice were intracranially inoculated with 90 000 GL261 cells as previously reported.<sup>[68]</sup> Mice were anesthetized by intraperitoneal injection of 100  $\mu\text{g g}^{-1}$  ketamine and 10  $\mu\text{g g}^{-1}$  xylazine and additionally medicated with 200  $\mu\text{g g}^{-1}$  metamizole (all from "Wirtschaftsgenossenschaft deutscher Tierärzte eG" (WDT), Garbsen, Germany). Mouse heads were fixed with a stereotactic frame (David Instruments, Tujanga, CA, USA) skulls were exposed by longitudinal skin incision and a hole was drilled 1.5 mm laterally and 1 mm anteriorly of the bregma using two microlances (BD Biosciences, Heidelberg, Germany). Cells suspended in 1.0  $\mu\text{L}$  phosphate buffered saline (PBS) were injected into the right striatum using a stereotactically guided Hamilton syringe (Hamilton, Bonaduz, Switzerland), skin was sutured, and mice were monitored till regaining consciousness. Tumor progression was monitored twice weekly by CBCT, starting at day 7 after inoculation as described.<sup>[26]</sup> For contrast enhancement, 300  $\mu\text{L}$  Imeron-300 (Bracco, Konstanz, Germany) was intravenously injected 3 min prior to CBCT. Tumor growth was assessed with measuring lengths, widths, and heights of tumors followed by spline regression. Irradiation was performed on a daily fractionation

regime over 2 weeks ( $2 \times 5 \times 2$  Gy) based on CBCT as described before.<sup>[26]</sup> The mouse VEGF-A-specific monoclonal antibody G6-31<sup>[35]</sup> was diluted to  $1 \text{ mg mL}^{-1}$  in PBS and was intraperitoneally injected at 0.1 mg of dose ( $0.1 \text{ mL}$  of  $1.0 \text{ mg mL}^{-1}$  dilution) at days 7, 11, and 14 after tumor inoculation. Vehicle controls received 0.1 mL PBS accordingly. Sacrificial of mice was performed by intraperitoneal injection of  $50 \mu\text{g g}^{-1}$  pentobarbital (WDT) and subsequent intracardial perfusion with cold PBS as described before.<sup>[26]</sup> Brains were explanted; tumors and contralateral samples of normal brain tissue were excised, snap-frozen in liquid nitrogen, and stored at  $-80^\circ\text{C}$  till further processing.

**Gene Expression Profiling of GL261 Tumors and Normal Mouse Brain Tissue:** Global mRNA expression profiling of GL261 tumors and normal brain tissue was performed by microarray analysis. Total RNA was extracted from excised tumors and normal brain tissue by NucleoSpin RNA II extraction kit (Macherey & Nagel, Dueren, Germany) and RNA quality was assessed by total RNA 6000 nano chip assay performed with an Agilent 2100 bioanalyzer (Agilent Technologies, Santa Clara, CA, USA). RNA was labeled with Cy3 and hybridized for 16 h at  $68^\circ\text{C}$  onto a  $4 \times 44 \text{ K}$  mouse gene expression microarray according the standard protocol (Agilent Technologies). Scanning of microarrays, data extraction, and preprocessing, including quality assessment and control were performed as described.<sup>[69]</sup>

**Molecular Subtyping of Orthotopically Implanted GL261 Tumors:** To assign GL261 tumors onto their respective molecular subtype, refined gene sets representing the transcriptomic profiles of each molecular subtype of human glioblastoma as published by Wang et al.<sup>[4]</sup> were adopted: for the mesenchymal subtype, the curated gene profile comprised the genes *RPC1B*, *S100A11*, *CTSC*, *GLIPR1*, *NNMT*, *VDR*, *RGS2*, *CTSB*, *TGFBI*, *PLAUR*, *LY96*, *BCL3*, *TNFAIP8*, *IER3*, *PRSS23*, *IL7R*, *RAB27A*, *RUNX1*, *P4HA2*, *CYP1B1*, *BACE2*, *ACPP*, *FTL*, *SLPI*, *RAC2*, *RARRES1*, *SYNGR2*, *THBS1*, *IL6*, *CAV1*, *PI3*, *CDCP1*, *ITGB1*, *LOX*, *COL1A1*, *COL1A2*, *COL3A1*, *COL5A1*, *CD72*, *ANPEP*, *MMP7*, *SPAG4*, *BNC2*, *NDRG1*, *CNN2*, *LUM*, *PTGS2*, *SDC1*, *GPRC5A*, and *COL15A1*. For the proneural subtype, the profile comprised genes *JPT1*, *RAB33A*, *HDAC2*, *MYT1*, *MTSS1*, *HOXD3*, *GPR17*, *PTTG1*, *KLRC3*, *PLAAT1*, *TCP1*, *NPPA*, *PFDN2*, *CA10*, *EPHB1*, *UGT8*, *PAK5*, *SLC1A1*, *NARF*, *DCTN3*, *SMPD3*, *ZNF804A*, *RASL11B*, *MYB*, *PDGFRA*, *ERBB3*, *CLGN*, *SOX10*, *BCL11A*, *NMU*, *ZNF643*, *CDKN1C*, *JPH3*, *PCDHA9*, *IL1RAPL1*, *MAST1*, *VIPR2*, *SIM2*, *BAMBI*, *PKMYT1*, *PLCB4*, *SLC17A6*, *KLRK1*, *CENPJ*, *NHLH1*, *GABRB3*, *KLRC4*, *KCNK3*, *GRID2*, and *DACH1*; and for classical subtype the profile comprised *PTPRA*, *ELOVL2*, *MLC1*, *SOX9*, *BMAL1*, *DENND2A*, *BBS1*, *ABLIM1*, *PAX6*, *ZHX3*, *USP8*, *PLCG1*, *CDH4*, *RASGRP1*, *ACSBG1*, *CST3*, *BCKDHB*, *LHFP*, *VAV3*, *ACSL3*, *EYA2*, *SEPT11*, *SLC4A4*, *SLC20A2*, *C14orf159*, *CTNND1*, *ZFH4*, *SPRY2*, *ZNF45*, *NCOA1*, *PLCE1*, *DTNA*, *POLRMT*, *SALL1*, *TYK2*, *TJP1*, *MEOX2*, *FGFR3*, *STXBP3*, *GRIK1*, *GATM*, *UPF1*, *NPEPL1*, *EFCAB14*, *RBCK1*, *PNPLA6*, *PPARGC1A*, *SLC3A2*, *PHKB*, and *MYO5C*. Translation of the human genes into homologous mouse (*mus musculus*) genes was performed with homogene (<https://www.ncbi.nlm.nih.gov/homologene>). NESs and enrichment plots comparing explanted GL261 tumors to normal murine brain tissue were calculated for each subtype-specific gene set using the fast GSEA (FGSEA) algorithm of the FGSEA package (version 1.22.0).<sup>[70]</sup> NESs of differently treated non-neoplastic brain tissues from the 50 hallmark genes encompassing MSigBD set<sup>[49]</sup> were derived in a similar fashion. To determine the expression of myeloid cell-specific gene signatures, custom gene sets for BMDMs, neutrophils, microglia, dendritic cells,  $\text{CD4}^+$  and  $\text{CD8}^+$  T cells, B cells, and NK cells were designed on the basis of microarray data from mouse leukocyte subsets obtained by the Immunological Genome (ImmGen) project (GSE15907 and GSE37448)<sup>[32]</sup> and using a non-negative matrix factorization (NMF) algorithm.<sup>[71]</sup> For discrimination between M1 and M2 polarization of macrophages, the gene sets published by Jablonski et al. were used.<sup>[33]</sup> NESs for all gene sets were calculated by FGSEA as described above and visualized by heat map clustering (Figure 3C).

**Analysis of TCGA-Derived Patient Data:** Transcriptomic data of 174 glioblastoma patients were obtained from the Broad Institute of the Massachusetts Institute of Technology (MIT) and the Harvard Firehose Initiative (<https://gdac.broadinstitute.org/>) and annotated to their respective molecular subtypes. PCA comparing transcriptomes in tumor samples with those in normal brain tissue was performed and paragon samples

corresponding to each molecular subtype were identified by FactoMineR (version 2.8).<sup>[72]</sup> KEGG<sup>[28]</sup> and GSEA<sup>[29]</sup> were performed with R (version 4.2.1) and RStudio (RStudio, PBC, Boston, MA, USA) and combined with gene set enrichment for pathway analysis (GAGE, version 2.48.0)<sup>[73]</sup> in case of KEGG, and FGSEA (version 1.22.0)<sup>[70]</sup> in case of GSEA. Single-sample gene set enrichment analyses (ssGSEAs) were performed using the gene set variation analysis (GSVA) package (version 1.44.5).<sup>[74]</sup> Statistical analyses, visualization of heatmaps, hierarchical clustering, as well as PCA, pie charts, and bar plots were performed with OriginPro (version 2021, OriginLab corporation, Northampton, MA, USA). Generation of annotated and clustered heatmaps was performed with complexHeatmap (version 2.12.1),<sup>[75]</sup> while functional interaction networks from preranked differential gene expression analyses (DEGs) were generated with Cytoscape (version 3.8.2).<sup>[76]</sup> Harmonization of human and mouse gene nomenclature was performed as described above.

**Statistical Analyses:** Tumor progression between treatment groups was compared by two-way analysis of variance (ANOVA) and mouse survival was analyzed by Kaplan–Meier curve analysis followed by log-rank test, both with Bonferroni–Holm correction.

## Supporting Information

Supporting Information is available from the Wiley Online Library or from the author.

## Acknowledgements

The authors thank Steffen Heuer and Laura Holler for technical assistance and Manfred Felbermeier for animal husbandry. This work was funded in part by a stipendium from the FoeFoLe program of the medical faculty of the “Ludwig-Maximilians-Universität” (LMU) Munich, Germany.

Open access funding enabled and organized by Projekt DEAL.

## Conflict of Interest

The authors declare no conflict of interest.

## Data Availability Statement

The data that support the findings of this study are available from the corresponding author upon reasonable request.

## Keywords

glioblastoma, inflammation, mesenchymal, normal brain tissue, radiotherapy, VEGF-A

Received: August 21, 2024

Revised: January 5, 2025

Published online: January 23, 2025

- [1] J. L. Fisher, J. A. Schwartzbaum, M. Wrensch, J. L. Wiemels, *Neurol. Clin.* **2007**, *25*, 867.
- [2] L. Rong, N. Li, Z. Z. Zhang, *J. Exp. Clin. Cancer Res.* **2022**, *41*, 142.
- [3] R. G. Verhaak, K. A. Hoadley, E. Purdom, V. Wang, Y. Qi, M. D. Wilkerson, C. R. Miller, L. Ding, T. Golub, J. P. Mesirov, G. Alexe, M. Lawrence, M. O’Kelly, P. Tamayo, B. A. Weir, S. Gabriel, W. Winckler, S. Gupta, L. Jakkula, H. S. Feiler, J. G. Hodgson, C. D. James, J. N. Sarkaria, C. Brennan, A. Kahn, P. T. Spellman, R. K. Wilson, T. P. Speed, J. W. Gray, M. Meyerson, et al., *Cancer Cell* **2010**, *17*, 98.

- [4] Q. Wang, B. Hu, X. Hu, H. Kim, M. Squatrito, L. Scarpace, A. C. deCarvalho, S. Lyu, P. Li, Y. Li, F. Barthel, H. J. Cho, Y. H. Lin, N. Satani, E. Martinez-Ledesma, S. Zheng, E. Chang, C. G. Sauve, A. Olar, Z. D. Lan, G. Finocchiaro, J. J. Phillips, M. S. Berger, K. R. Gabrusiewicz, G. Wang, E. Eskilsson, J. Hu, T. Mikkelsen, R. A. DePino, F. Muller, et al., *Cancer Cell* **2017**, *32*, 42.
- [5] K. P. L. Bhat, V. Balasubramanian, B. Vaillant, R. Ezhilarasan, K. Hummelink, F. Hollingsworth, K. Wani, L. Heathcock, J. D. James, L. D. Goodman, S. Conroy, L. H. Long, N. Lelic, S. Z. Wang, J. Gumin, D. Raj, Y. Kodama, A. Raghunathan, A. Olar, K. Joshi, C. E. Pelloski, A. Heimberger, S. H. Kim, D. P. Cahill, G. Rao, W. F. A. Den Dunnen, H. W. G. M. Boddeke, H. S. Phillips, L. Nakano, F. F. Lang, et al., *Cancer Cell* **2013**, *24*, 331.
- [6] Z. Azam, S. S. T. To, B. A. Tannous, *Adv. Sci.* **2020**, *7*, 2002015.
- [7] N. Ferrara, K. J. Hillan, W. Novotny, *Biochem. Biophys. Res. Commun.* **2005**, *333*, 328.
- [8] A. D. Norden, J. Drappatz, P. Y. Wen, *Nat. Rev. Neurol.* **2009**, *5*, 610.
- [9] O. L. Chinot, W. Wick, W. Mason, R. Henriksson, F. Saran, R. Nishikawa, A. F. Carpentier, K. Hoang-Xuan, P. Kavan, D. Cernea, A. A. Brandes, M. Hilton, L. Abrey, T. Cloughesy, *N. Engl. J. Med.* **2014**, *370*, 709.
- [10] M. R. Gilbert, J. J. Dignam, T. S. Armstrong, J. S. Wefel, D. T. Blumenthal, M. A. Vogelbaum, H. Colman, A. Chakravarti, S. Pugh, M. Won, R. Jeraj, P. D. Brown, K. A. Jaeckle, D. Schiff, V. W. Stieber, D. G. Brachman, M. Werner-Wasik, I. W. Tremont-Lukats, E. P. Sulman, K. D. Aldape, W. J. Curran, M. P. Mehta, *N. Engl. J. Med.* **2014**, *370*, 699.
- [11] W. Wick, T. Gorlia, M. Bendszus, M. Taphoorn, F. Sahm, I. Harting, A. A. Brandes, W. Taal, J. Domont, A. Idbaih, M. Campone, P. M. Clement, R. Stupp, M. Fabbro, E. Le Rhun, F. Dubois, M. Weller, A. von Deimling, V. Gofinopoulos, J. C. Bromberg, M. Platten, M. Klein, M. J. van den Bent, *N. Engl. J. Med.* **2017**, *377*, 1954.
- [12] T. Sandmann, R. Bourgon, J. Garcia, C. F. Li, T. Cloughesy, O. L. Chinot, W. Wick, R. Nishikawa, W. Mason, R. Henriksson, F. Saran, A. Lai, N. Moore, S. Kharbanda, F. Peale, P. Hegde, L. E. Abrey, H. S. Phillips, C. Bais, *J. Clin. Oncol.* **2015**, *33*, 2735.
- [13] A. Scherm, F. M. Ippen, P. Hau, H. Baurecht, W. Wick, J. Gempt, H. Knüttel, M. F. Leitzmann, C. Seliger, *Int. J. Cancer* **2023**, *152*, 2373.
- [14] M. Weller, M. van den Bent, M. Preusser, E. Le Rhun, J. C. Tonn, G. Minniti, M. Bendszus, C. Balana, O. Chinot, L. Dirven, P. French, M. E. Hegi, A. S. Jakola, M. Platten, P. Roth, R. Rudà, S. Short, M. Smits, M. J. B. Taphoorn, A. von Deimling, M. Westphal, R. Soffietti, G. Reifenberger, W. Wick, *Nat. Rev. Clin. Oncol.* **2022**, *19*, 357.
- [15] H. S. Friedman, M. D. Prados, P. Y. Wen, T. Mikkelsen, D. Schiff, L. E. Abrey, W. K. A. Yung, N. Paleologos, M. K. Nicholas, R. Jensen, J. Vredenburgh, J. Huang, M. X. Zheng, T. Cloughesy, *J. Clin. Oncol.* **2009**, *27*, 4733.
- [16] M. J. Fu, Z. R. Zhou, X. Huang, Z. C. Chen, L. C. Zhang, J. S. Zhang, W. Hua, Y. Mao, *BMC Cancer* **2023**, *23*, 544.
- [17] K. E. Hovinga, H. J. McCrea, C. Brennan, J. Huse, J. T. Zheng, Y. Esquenazi, K. S. Panageas, V. Tabar, *J. Neuro-Oncol.* **2019**, *142*, 337.
- [18] J. Weller, T. Zeyen, N. Schafer, C. Schaub, A. L. Potthoff, J. P. Steinbach, P. Hau, C. Seidel, R. Goldbrunner, G. Tabatabai, H. Vatter, T. Tzaridis, M. Schneider, U. Herrlinger, *J. Neurooncol.* **2023**, *164*, 749.
- [19] A. A. Dmytriw, R. Y. Huang, *Neuro-Oncology* **2021**, *23*, 184.
- [20] C. I. Tsien, S. L. Pugh, A. P. Dicker, J. J. Raizer, M. M. Matuszak, E. C. Lallana, J. Huang, O. Algan, N. Deb, L. Portelance, J. L. Villano, J. T. Hamm, K. S. Oh, A. N. Ali, M. M. Kim, S. M. Lindhorst, M. P. Mehta, *J. Clin. Oncol.* **2023**, *41*, 1285.
- [21] M. Flieger, U. Ganswindt, S. B. Schwarz, F. W. Kreth, J. C. Tonn, C. la Fougère, L. Ertl, J. Linn, U. Herrlinger, C. Belka, M. Niyazi, *J. Neuro-Oncol.* **2014**, *117*, 337.
- [22] J. I. Ausman, W. R. Shapiro, D. P. Rall, *Cancer Res.* **1970**, *30*, 2394.
- [23] V. A. Levin, L. Bidaut, P. Hou, A. J. Kumar, J. S. Wefel, B. N. Bekele, S. Prabhu, M. Loghin, M. R. Gilbert, E. F. Jackson, *Int. J. Radiat. Oncol., Biol., Phys.* **2011**, *79*, 1487.
- [24] D. F. Fleischmann, J. Jenn, S. Corradini, V. Ruf, J. Herms, R. Forbrügge, M. Unterrainer, N. Thon, F. W. Kreth, C. Belka, M. Niyazi, *Radiother. Oncol.* **2019**, *138*, 99.
- [25] R. Bodensohn, I. Hadi, D. F. Fleischmann, S. Corradini, N. Thon, J. Rauch, C. Belka, M. Niyazi, *Strahlenther. Onkol.* **2020**, *196*, 70.
- [26] B. Stegen, A. Nieto, V. Albrecht, J. Maas, M. Orth, K. Neumaier, S. Reinhardt, M. Weick-Kleemann, W. Goetz, M. Reinhart, K. Parodi, C. Belka, M. Niyazi, K. Lauber, *Radiat. Oncol.* **2020**, *15*, 19.
- [27] J. N. Weinstein, E. A. Collisson, G. B. Mills, K. R. M. Shaw, B. A. Ozenberger, K. Ellrott, I. Shmulevich, C. Sander, J. M. Stuart, The Cancer Genome Atlas Research Network, *Nat. Genet.* **2013**, *45*, 1113.
- [28] H. Ogata, S. Goto, K. Sato, W. Fujibuchi, H. Bono, M. Kanehisa, *Nucleic Acids Res.* **1999**, *27*, 29.
- [29] A. Subramanian, P. Tamayo, V. K. Mootha, S. Mukherjee, B. L. Ebert, M. A. Gillette, A. Paulovich, S. L. Pomeroy, T. R. Golub, E. S. Lander, J. P. Mesirov, *Proc. Natl. Acad. Sci. USA* **2005**, *102*, 15545.
- [30] I. Kaffes, F. Szulzewsky, Z. H. Chen, C. J. Herting, B. Gabanic, J. E. V. Vega, J. Shelton, J. M. Switchenko, J. L. Ross, L. F. McSwain, J. T. Huse, B. Westermarck, S. Nelander, K. Forsberg-Nilsson, L. Uhrbom, N. P. Maturi, P. J. Cimino, E. C. Holland, H. Kettenmann, C. W. Brennan, D. J. Brat, D. Hambarzumyan, *Oncoimmunology* **2019**, *8*, e1655360.
- [31] T. Hara, R. Chanoch-Myers, N. D. Mathewson, C. Myskiw, L. Atta, L. Bussema, S. W. Eichhorn, A. C. Greenwald, G. S. Kinker, C. Rodman, L. N. Gonzalez Castro, H. Wakimoto, O. Rozenblatt-Rosen, X. Zhuang, J. Fan, T. Hunter, I. M. Verma, K. W. Wucherpfennig, A. Regev, M. L. Suvà, I. Tirosh, *Cancer Cell* **2021**, *39*, 779.
- [32] T. S. P. Heng, M. W. Painter, I. G. Project, *Nat. Immunol.* **2008**, *9*, 1091.
- [33] K. A. Jablonski, S. A. Amici, L. M. Webb, J. D. Ruiz-Rosado, P. G. Popovich, S. Partida-Sanchez, M. Guerau-de-Arellano, *PLoS One* **2015**, *10*, e0145342.
- [34] M. G. Huang, D. Zhang, J. Y. Wu, K. Xing, E. J. Yeo, C. S. Li, L. Zhang, E. Holland, L. T. Yao, L. Qin, Z. A. Binder, D. M. O'Rourke, S. Brem, C. Koumenis, Y. Q. Gong, Y. Fan, *Sci. Transl. Med.* **2020**, *12*, eaay7522.
- [35] W. C. Liang, X. M. Wu, F. V. Peale, C. V. Lee, G. Meng, J. Gutierrez, L. Fu, A. K. Malik, H. P. Gerber, N. Ferrara, G. Fuh, *J. Biol. Chem.* **2006**, *281*, 951.
- [36] F. Winkler, S. V. Kozin, R. T. Tong, S. S. Chae, M. F. Booth, I. Garkavtsev, L. Xu, D. J. Hicklin, D. Fukumura, E. di Tomaso, L. L. Munn, R. K. Jain, *Cancer Cell* **2004**, *6*, 553.
- [37] P. R. Wachsberger, R. Burd, C. Cardi, M. Thakur, C. Daskalakis, J. Holash, G. D. Yancopoulos, A. P. Dicker, *Int. J. Radiat. Oncol., Biol., Phys.* **2007**, *67*, 1526.
- [38] J. J. C. Verhoeff, L. J. A. Stalpers, A. Claes, K. E. Hovinga, G. D. Musters, W. P. Vandertop, D. J. Richel, W. P. J. Leenders, W. R. van Furth, *Eur. J. Cancer* **2009**, *45*, 3074.
- [39] J. Halliday, K. Helmy, S. S. Pattwell, K. L. Pitter, Q. LaPlant, T. Ozawa, E. C. Holland, *Proc. Natl. Acad. Sci. USA* **2014**, *111*, 5248.
- [40] Y. Piao, J. Liang, L. Holmes, V. Henry, E. Sulman, J. F. de Groot, *Clin. Cancer Res.* **2013**, *19*, 4392.
- [41] E. K. Nduom, M. Weller, A. B. Heimberger, *Neuro-Oncology* **2015**, *17*, vii9.
- [42] M. Rydenfelt, B. Klingner, M. Klünemann, N. Blüthgen, *Nucleic Acids Res.* **2020**, *48*, W307.
- [43] N. Nonoguchi, S. I. Miyatake, M. Fukumoto, M. Furuse, R. Hiramatsu, S. Kawabata, T. Kuroiwa, M. Tsuji, M. Fukumoto, K. Ono, *J. Neuro-Oncol.* **2011**, *105*, 423.
- [44] S. Schumacher, H. Tahiri, P. Ezan, N. Rouach, K. Witschas, L. Leybaert, *Glia* **2023**, *72*, 34.

- [45] A. T. Argaw, L. Asp, J. Y. Zhang, K. Navrazhina, T. Pham, J. N. Mariani, S. Mahase, D. J. Dutta, J. Seto, E. G. Kramer, N. Ferrara, M. V. Sofroniew, G. R. John, *J. Clin. Invest.* **2012**, *122*, 2454.
- [46] C. Chapouly, A. T. Argaw, S. Horng, K. Castro, J. Y. Zhang, L. Asp, H. Loo, B. M. Laitman, J. N. Mariani, R. S. Farber, E. Zaslavsky, G. Nudelman, C. S. Raine, G. R. John, *Brain* **2015**, *138*, 1548.
- [47] S. Michinaga, A. Kimura, S. Hatanaka, S. Minami, A. Asano, Y. Ikushima, S. Matsui, Y. Toriyama, M. Fujii, Y. Koyama, *J. Neurotrauma* **2018**, *35*, 1481.
- [48] M. Niklasson, T. Bergström, M. Jarvius, A. Sundström, F. Nyberg, C. Haglund, R. Larsson, B. Westermark, B. Segerman, A. Segerman, *J. Pathol.* **2019**, *249*, 295.
- [49] A. Liberzon, A. Subramanian, R. Pinchback, H. Thorvaldsdóttir, P. Tamayo, J. P. Mesirov, *Bioinformatics* **2011**, *27*, 1739.
- [50] A. C. Tan, D. M. Ashley, G. Y. López, M. Malinzak, H. S. Friedman, M. Khasraw, *ca-Cancer J. Clin.* **2020**, *70*, 299.
- [51] I. J. Barani, D. A. Larson, *Cancer Treat. Res.* **2015**, *163*, 49.
- [52] S. Osuka, E. G. Van Meir, *J. Clin. Invest.* **2017**, *127*, 415.
- [53] J. D. Ruben, M. Dally, M. Bailey, R. Smith, C. A. McLean, P. Fedele, *Int. J. Radiat. Oncol., Biol., Phys.* **2006**, *65*, 499.
- [54] R. J. Diaz, S. Ali, M. G. Qadir, M. I. De la Fuente, M. E. Ivan, R. J. Komotar, *J. Neuro-Oncol.* **2017**, *133*, 455.
- [55] C. Garcia, L. G. Dubois, A. L. Xavier, L. H. Geraldo, A. C. C. da Fonseca, A. H. Correia, F. Meirelles, G. Ventura, L. Romao, N. H. S. Canedo, J. M. de Souza, J. R. L. de Menezes, V. Moura-Neto, F. Tovar-Moll, F. R. S. Lima, *BMC Cancer* **2014**, *14*, 923.
- [56] A. Frisch, S. Kälin, R. Monk, J. Radke, F. L. Heppner, R. E. Kälin, *Int. J. Mol. Sci.* **2020**, *21*, 4179.
- [57] T. N. Kreisl, L. Kim, K. Moore, P. Duic, C. Royce, I. Stroud, N. Garren, M. Mackey, J. A. Butman, K. Camphausen, J. Park, P. S. Albert, H. A. Fine, *J. Clin. Oncol.* **2009**, *27*, 740.
- [58] L. Wang, J. Jung, H. Babikir, K. Shamardani, S. Jain, X. Feng, N. Gupta, S. Rosi, S. Chang, D. Raleigh, D. Solomon, J. J. Phillips, A. A. Diaz, *Nat. Cancer* **2022**, *3*, 1534.
- [59] B. N. Nandeesh, S. Naskar, A. H. Shashtri, A. Arivazhagan, V. Santosh, *J. Neurosci. Rural Pract.* **2018**, *9*, 86.
- [60] L. She, L. Su, C. Liu, *Front. Oncol.* **2022**, *12*, 961014.
- [61] W. C. You, H. D. Lee, H. C. Pan, H. C. Chen, *Sci. Rep.* **2023**, *13*, 9442.
- [62] E. V. Mitroshina, M. Saviuk, M. V. Vedunova, *Front. Aging Neurosci.* **2023**, *14*, 1016053.
- [63] K. Lumniczky, T. Szatmári, G. Sáfrány, *Front. Immunol.* **2017**, *8*, 517.
- [64] D. Boothe, R. Young, Y. Yamada, A. Prager, T. Chan, K. Beal, *Neuro-Oncology* **2013**, *15*, 1257.
- [65] M. Khan, Z. H. Zhao, S. Arooj, G. X. Liao, *BMC Cancer* **2021**, *21*, 167.
- [66] J. Li, J. He, L. B. Cai, M. Y. Lai, Q. J. Hu, C. Ren, L. Wen, J. Wang, J. F. Zhou, Z. M. Zhou, S. Q. Li, M. T. Ye, C. G. Shan, L. H. Chen, C. Zhou, *Ann. Palliat. Med.* **2021**, *10*, 2018.
- [67] J. Tijtgat, E. Calliauw, I. Dirven, M. Vounckx, R. Kamel, A. M. Vanbinst, H. Everaert, L. Seynaeve, D. Van Den Berge, J. Duerinck, B. Neyns, *Cancers* **2023**, *15*, 2560.
- [68] M. Orth, V. Albrecht, K. Seidl, L. Kinzel, K. Unger, J. Hess, L. Kreutzer, N. Sun, B. Stegen, A. Nieto, J. Maas, N. Winssinger, A. A. Friedl, A. K. Walch, C. Belka, H. Zitzelsberger, M. Niyazi, K. Lauber, *Front. Oncol.* **2021**, *11*, 612354.
- [69] C. M. Wilke, J. Hess, S. V. Klymenko, V. V. Chumak, L. M. Zakhartseva, E. V. Bakhanova, A. Feuchtinger, A. K. Walch, M. Selmansberger, H. Braselmann, L. Schneider, A. Pitea, J. Steinhilber, F. Fend, H. C. Bösmüller, H. Zitzelsberger, K. Unger, *Int. J. Cancer* **2018**, *142*, 573.
- [70] G. Korotkevich, V. Sukhov, N. Budin, B. Shpak, M. N. Artyomov, A. Sergushichev, *bioRxiv: 060012* **2021**.
- [71] Y. Liao, G. K. Smyth, W. Shi, *Bioinformatics* **2014**, *30*, 923.
- [72] S. Lê, J. Josse, F. Husson, *J. Stat. Software* **2008**, *25*, 1.
- [73] W. J. Luo, M. S. Friedman, K. Shedden, K. D. Hankenson, P. J. Woolf, *BMC Bioinf.* **2009**, *10*, 161.
- [74] S. Hänzelmann, R. Castelo, J. Guinney, *BMC Bioinf.* **2013**, *14*, 7.
- [75] Z. G. Gu, R. Eils, M. Schlesner, *Bioinformatics* **2016**, *32*, 2847.
- [76] P. Shannon, A. Markiel, O. Ozier, N. S. Baliga, J. T. Wang, D. Ramage, N. Amin, B. Schwikowski, T. Ideker, *Genome Res.* **2003**, *13*, 2498.